A Newton Method for the Resolution of Steady Stochastic Navier-Stokes Equations☆

Olivier Le Maître[a,b,*]

[a] *LIMSI-CNRS*
[b] *CEA/DEN/DM2S, centre de Saclay*

Abstract

We present a Newton method to compute the stochastic solution of the steady incompressible Navier-Stokes equations with random data (boundary conditions, forcing term, fluid properties). The method assumes a spectral discretization at the stochastic level involving a orthogonal basis of random functionals (such as Polynomial Chaos or stochastic multiwavelets bases). The Newton method uses the unsteady equations to derive a linear equation for the stochastic Newton increments. This linear equation is subsequently solved following a matrix-free strategy, where the iterations consist in performing integrations of the linearized unsteady Navier-Stokes equations, with an appropriate time scheme to allow for a decoupled integration of the stochastic modes. Various examples are provided to demonstrate the efficiency of the method in determining stochastic steady solution, even for regimes where it is likely unstable.

Key words: Uncertainty quantification, steady flow, stochastic spectral method, Newton iterations

1. Introduction

Many fluid flow simulations involve incomplete knowledge of model input, such as physical constants and fluid properties, boundary and initial conditions, external forcing,... Quantifying the impact of these uncertainties on the model output is crucial to assess confidence level, to estimate variability and limits of predictability, and to support any model-based decision analysis.

Among the various techniques that have been designed for the purpose of uncertainty propagation and quantification in numerical models, the so-called stochastic spectral methods have received considerable and growing attention over the last ten years. These probabilistic methods were originally developed for engineering problems in solid mechanics [10] and subsequently applied to a large variety of problems, including elliptic models and flow/transport in porous media (*e.g.* [8, 9, 2, 15, 25]), thermal problems (*e.g.* [11, 12, 24]) and reacting systems (*e.g* [6, 28, 21]). The core idea of these techniques is the representation of the uncertain model data as functionals of a finite set of random variables with known densities, the uncertainty germ, and to expand the dependence of the model solution, with regard to the same random variables, on a suitable basis of uncorrelated functionals of the germs. By essence, these methods are parametric and so are limited to uncertainties that one can reasonably parameterize (this exclude model uncertainty which requires a non parametric framework [32, 33]).

A classical and historical choice for the expansion basis is the Polynomial Chaos system [39, 3], consisting of orthogonal Hermite polynomials in normalized centered Gaussian random variables [10]. Other density types for the germ components result in various families of orthogonal polynomials or mixtures of orthogonal

☆This work is supported by the ANR, Project ASRMEI, grant number JC08-375619
*LIMSI-CNRS, BP133, F-91403 ORSAY cedex, France
Email addresses: olm@limsi.fr (Olivier Le Maître)
URL: http://www.limsi.fr/Individu/olm (Olivier Le Maître)

polynomials [40]. First applications of PC methods to Eulerian formulations of the incompressible Navier-Stokes equations appeared in [18, 22, 41], to Low-Mach approximation in [16], while Lagrangian formulations were recently considered in [17]. Note that use of non-Gaussian germs in fluid flow models was first considered in [41]. A review of recent works using PC expansions in Navier-Stokes computations can be found in [14]. Piecewise polynomials [38] and multi-wavelets [19, 20] were also recently proposed as elements of the basis, as these representations are better suited to account for complex or discontinuous dependencies of the model with regard to the uncertain data, as often encountered in fluid flow.

The present paper is in the continuity of these past efforts toward the application of stochastic spectral methods to fluid flow models. It describes a Newton method to efficiently solve the spectral problems arising from the Galerkin projection of the steady stochastic Navier-Stokes equations. It is a direct extension of the techniques originally designed for deterministic problems [35, 7, 36]. The method is particularly appealing in the stochastic spectral context as it requires little modifications of the unsteady stochastic solver, while preserving it essential characteristic: the decoupled resolution of the stochastic modes.

The paper is organized as follow. In Section 2 we recall the incompressible Navier-Stokes equations and introduce some notations and the class of time discretization schemes to be used in the Newton method. In Section 3, the stochastic framework in progressively introduced, leading to the numerical method for the integration of the unsteady stochastic Navier-Stokes equations. Special emphasize is on the time-discretizations that decouple the integration of the spectral modes. Section 4 concerns the Newton method for the resolution of the stochastic steady Navier-Stokes equations. The Newton iterations, together with the equations satisfied by the Newton increments, are detailed before discussing the matrix-free technique for their computation. The Newton method is then tested in Sections 5 and 6 where we provide examples of increasing stochastic dimension and complexity. These examples are used to assess the efficiency and robustness of the Newton iterations with regard to numerical and discretization parameters, flow variability and stability of the stochastic steady solution. Finally, major conclusions of this work and recommendations are drawn in Section 7.

2. Navier-Stokes equations

We consider the flow of an incompressible Newtonian fluid, with uniform density and kinematic viscosity ν, in a d-dimensional bounded domain Ω_x of $\mathbb{R}^d$. The flow is governed by the dimensionless unsteady Navier-Stokes equations

$$\left\{ \begin{array}{l} \dfrac{\partial \boldsymbol{u}}{\partial t} + \boldsymbol{u} \cdot (\boldsymbol{\nabla} \boldsymbol{u}) = -\boldsymbol{\nabla} p + \dfrac{1}{\mathrm{Re}} \nabla^2 \boldsymbol{u} + \boldsymbol{f}, \\ \boldsymbol{\nabla} \cdot \boldsymbol{u} = 0, \end{array} \right. \tag{1}$$

where $\boldsymbol{u}$ and p are the dimensionless velocity and pressure, $\boldsymbol{f}$ is a normalized force field and $\mathrm{Re} = U_c L_c / \nu$ is the Reynolds number based on the characteristic velocity and length scales U_c and L_c. These equations have to be complemented with initial conditions, say at $t = 0$, and boundary conditions on Γ, the boundary of Ω_x. Without loss of generality, we shall consider Dirichlet boundary conditions so boundary and initial conditions are

$$\left\{ \begin{array}{l} \boldsymbol{u}(\boldsymbol{x} \in \Gamma, t) = \boldsymbol{u}_\Gamma(\boldsymbol{x}), \\ \boldsymbol{u}(\boldsymbol{x}, t = 0) = \boldsymbol{u}_0(\boldsymbol{x}). \end{array} \right. \tag{2}$$

Note that we restrict ourself to time independent boundary conditions, as we are interested in steady solutions in the following. For the resolution of Eqs. (1), we focus on time discretizations involving an explicit treatment of the non-linear terms and an implicit (or semi-implicit) treatment of the linear ones. For simplicity, we consider a simple first order Euler scheme:

$$\left\{ \begin{array}{r} \left(\boldsymbol{I} - \dfrac{\Delta t}{\mathrm{Re}} \boldsymbol{\nabla}^2 \right) \boldsymbol{u}^{n+1} + \Delta t \boldsymbol{\nabla} p^{n+1} = \boldsymbol{u}^n - \Delta t \boldsymbol{u}^n \cdot \boldsymbol{\nabla} \boldsymbol{u}^n + \Delta t \boldsymbol{f}^{n+1}, \\ \boldsymbol{\nabla} \cdot \boldsymbol{u}^{n+1} = 0, \end{array} \right. \tag{3}$$

where the superscripts refer to the time-iteration index and Δt is the time-step size. It is seen that this time-discretization, as any other where the non-linear terms are treated explicitly, results in a linear problem (namely the Stokes problem) for the unknown solution at time level $n + 1$.

The main difficulty faced when solving the semi-discrete Navier-Stokes system (3) is due to the divergence free constraint. For formulations using primitive variables (velocity and pressure), several strategies have been proposed to enforce the divergence-free constraint on the solution, *e.g.* the projection methods [4, 13], Uzawa techniques and influence matrix methods [5, 37]. It is known that some strategies provide discrete solutions that satisfy exactly the boundary conditions (*e.g* the influence matrix), while others only approximatively satisfy the boundary conditions (*e.g.* the projection methods). Alternative formulations, *e.g.* stream-function vorticity formulations, overcome the difficulty inherent to the enforcement of the divergence-free constraint, but face the difficulty of the absence of natural boundary conditions. Again, one can rely on approximate or exact techniques to determine the unknown boundary conditions.

To remain as general as possible, we recast the semi-discrete Navier-Stokes equations (3) in the following formal expression:

$$\mathcal{I}\left(\mathcal{U}^{n+1}\right) = \mathcal{L}(\mathcal{U}^n, \mathcal{U}^{n-1}, \ldots) + \mathcal{N}\left(\mathcal{U}^n, \mathcal{U}^{n-1}, \ldots\right) + \mathcal{S}(\boldsymbol{f}^{n+1}), \tag{4}$$

where $\mathcal{U}^{n+1}$ is the sought solution at time $t = (n+1)\Delta t$. Eq. (4) has to be solved for $\mathcal{U}^{n+1} \in \mathscr{V}_{\boldsymbol{u}_\Gamma}$, where $\mathscr{V}_{\boldsymbol{u}_\Gamma}$ is a suitable functional space for $\mathcal{U}$ satisfying the boundary conditions. In fact, Eq. (4) relates the solution at time level $n+1$ (appearing on the left-hand-side) to the (known) solutions at previous time levels (n, $n-1$, ...). Moreover, $\mathcal{I}$ and $\mathcal{L}$ are linear operators, while $\mathcal{N}$ is a non-linear operator. The last term $\mathcal{S}$ accounts for the force field. We assume the availability of a deterministic solver for the resolution of Eq. (4). In addition, we shall consider in the following Eq. (4) as a generic form of the semi-discrete incompressible Navier-Stokes equations, where the formal notation $\mathcal{U}$ of the solution stands for the relevant set of variables involved in the actual formulation, so that $\mathcal{U} = (\boldsymbol{u}, p)$ in primitive variables formulations, $\mathcal{U} = (\omega)$ in vorticity formulations, $\mathcal{U} = (\omega, T)$ when the Navier-Stokes equations are complemented with an energy equation (see Boussinesq example below).

3. Stochastic spectral expansions

3.1. Probabilistic framework

We now consider the stochastic problem. For the sake of simplicity, we restrict ourselves temporarily to situations where the uncertainty arises from random boundary conditions and source term. To solve the uncertain flow, we rely on a probabilistic framework and introduce an abstract probability space $(\Theta, \mathcal{B}, dP)$, where Θ is the set of random events, $\mathcal{B}$ is the σ-algebra of events and dP the probability measure. Let $h(\theta)$ be a real-valued random variable defined on the abstract probability space: $h : \theta \in \Theta \mapsto f(\theta) \in \mathbb{R}$. We denote $E(\cdot)$ the mathematical expectation,

$$E(h) \equiv \int_\Theta h(\theta) dP(\theta), \tag{5}$$

and $L^2(\Theta, dP)$ the space of second order random variables:

$$L^2(\Theta, dP) \equiv \left\{h(\theta); E(h^2) < +\infty\right\}. \tag{6}$$

We shall assume in the following that all random quantities (scalars and vectors) are second order ones. We further assume a parameterization of the random boundary conditions and source term using a finite set $\boldsymbol{\xi} \equiv \{\xi_1, \ldots, \xi_\mathrm{N}\}$ of N independent continuous real-valued random variables defined on $(\Theta, \mathcal{B}, dP)$ (for non independent random variables see [34]). We denote $\Omega_{\boldsymbol{\xi}}$ the range of $\boldsymbol{\xi}$. For convenience, the random variables ξ_i will be identically distributed and we denote $P_{\boldsymbol{\xi}}$ the probability law of $\boldsymbol{\xi}$. In the image probability space $(\Omega_{\boldsymbol{\xi}}, \mathcal{B}_{\boldsymbol{\xi}}, dP_{\boldsymbol{\xi}})$ the expectation operator becomes

$$E(h) = \int_\Theta h(\theta) dP(\theta) = \int_{\Omega_{\boldsymbol{\xi}}} h(\boldsymbol{\eta}) dP_{\boldsymbol{\xi}}(\boldsymbol{\eta}) d\boldsymbol{\eta} \equiv \langle h \rangle. \tag{7}$$

The parameterization of the boundary condition and source term are

$$\boldsymbol{u}_\Gamma(\theta) = \boldsymbol{u}_\Gamma(\boldsymbol{\xi}(\theta)), \quad \boldsymbol{f}(\theta) = \boldsymbol{f}(\boldsymbol{\xi}(\theta)), \tag{8}$$

and the solution $\mathcal{U}$ is sought in the image probability space, *i.e.* we compute $\mathcal{U}(\boldsymbol{\xi})$.

3.2. Stochastic discretization

Let $\{\Psi_i(\boldsymbol{\xi})\}_{i=0}^{i=\infty}$ be an orthogonal basis of $L^2(\Omega_{\boldsymbol{\xi}}, dP_{\boldsymbol{\xi}})$, the space of second order random variables spanned by $\boldsymbol{\xi}$. The orthogonality of the basis functions reads:

$$\langle \Psi_i \Psi_j \rangle = \int_{\Omega_{\boldsymbol{\xi}}} \Psi_i(\boldsymbol{y}) \Psi_j(\boldsymbol{y}) dP_{\boldsymbol{\xi}}(\boldsymbol{y}) d\boldsymbol{y} = \left\langle \Psi_i^2 \right\rangle \delta_{ij}. \tag{9}$$

On this basis, the stochastic expansion of the velocity boundary condition is

$$\boldsymbol{u}_\Gamma(\boldsymbol{\xi}) = \sum_{i=0}^{\infty} (\boldsymbol{u}_\Gamma)_i \, \Psi_i(\boldsymbol{\xi}), \quad (\boldsymbol{u}_\Gamma)_i = \frac{\langle \boldsymbol{u}_\Gamma(\boldsymbol{\xi}) \Psi_i(\boldsymbol{\xi}) \rangle}{\langle \Psi_i \Psi_i \rangle}. \tag{10}$$

The expansion of the force field is similar. A classical choice for the stochastic expansion basis is the set of orthogonal polynomials in $\boldsymbol{\xi}$. When the ξ_i are normalized Gaussian random variables the Ψ_i are in fact Hermite polynomials, while uniform distributions correspond to Legendre polynomials [1]. Families of orthogonal polynomials for classical probability distributions can be found in [40]. The construction of an orthogonal basis for independent non-identically distributed random variables is immediate, by forming multi-dimensional polynomials as product (mixture) of different families of one-dimensional polynomials. The case of non independent random variables was considered in [34] and leads to non-polynomial orthogonal bases. Alternatives for the construction of the stochastic basis are multi-wavelets [19, 20] or piecewise continuous polynomials [38]. The developments hereafter extend without conceptual difficulty to any type of orthogonal basis.

3.3. Stochastic spectral problem

The Navier-Stokes equations now involving random quantities they have a random solution with formal expansion

$$\mathcal{U}(\theta) = \mathcal{U}(\boldsymbol{\xi}(\theta)) = \sum_{i=0}^{\infty} (\mathcal{U})_i \, \Psi_i(\boldsymbol{\xi}(\theta)) \in \mathscr{V}_{\boldsymbol{u}_\Gamma} \otimes L^2(\Omega_{\boldsymbol{\xi}}, dP_{\boldsymbol{\xi}}). \tag{11}$$

Introducing the solution expansion in Eq. (4), it comes

$$\begin{aligned} \mathcal{I}\left(\sum_i \left(\mathcal{U}^{n+1}\right)_i \Psi_i \right) &= \mathcal{L}\left(\sum_i \left(\mathcal{U}^{n}\right)_i \Psi_i, \sum_i \left(\mathcal{U}^{n-1}\right)_i \Psi_i, \dots \right) \\ &+ \mathcal{N}\left(\sum_i \left(\mathcal{U}^{n}\right)_i \Psi_i, \sum_i \left(\mathcal{U}^{n-1}\right)_i \Psi_i, \dots \right) \\ &+ \mathcal{S}\left(\sum_i \left(\boldsymbol{f}^{n+1}\right)_i \Psi_i \right). \end{aligned} \tag{12}$$

To solve Eq. (12), the stochastic expansion has to be truncated. To remain general with regard to the stochastic discretization used, we denote

$$\mathscr{S}^{\mathrm{P}} \equiv \mathrm{span}\{\Psi_0, \dots, \Psi_{\mathrm{P}}\} \subset L^2(\Omega_{\boldsymbol{\xi}}, dP_{\boldsymbol{\xi}}) \tag{13}$$

the finite dimensional stochastic approximation space with $\dim(\mathscr{S}^{\mathrm{P}}) = \mathrm{P} + 1$. For continuous polynomial bases, the truncature is usually made by fixing a maximal (total) degree No for the polynomials spanning $\mathscr{S}^{\mathrm{P}}$ so in this case [10]:

$$\mathrm{P} + 1 = (\mathrm{No} + \mathrm{N})!/(\mathrm{No}!\mathrm{N}!). \tag{14}$$

Substituting $\mathcal{U}$ with its truncated expansion, Eq. (12) is not satisfied in general, but yields a stochastic residual. A weak solution of the problem is then sought by requiring the residual to be orthogonal to $\mathscr{S}^{\mathrm{P}}$.

With this constraint, it comes for $i = 0, \ldots, \mathrm{P}$

$$\begin{aligned}\left\langle \Psi_i \mathcal{I} \left(\sum_{j=0}^{\mathrm{P}} (\mathcal{U})_j^{n+1} \Psi_j \right) \right\rangle &= \left\langle \Psi_i \mathcal{L} \left(\sum_{j=0}^{\mathrm{P}} (\mathcal{U})_j^{n} \Psi_j \right) \right\rangle + \left\langle \Psi_i \mathcal{N} \left(\sum_{j=0}^{\mathrm{P}} (\mathcal{U})_j^{n} \Psi_j \right) \right\rangle \\ &+ \left\langle \Psi_i \mathcal{S} \left(\sum_{j=0}^{\mathrm{P}} \left(\boldsymbol{f}^{n+1}\right)_j \Psi_j, \right) \right\rangle, \end{aligned} \tag{15}$$

to be solve for $\mathcal{U}^{n+1} \in \mathscr{V}_{\boldsymbol{u}_\Gamma} \otimes \mathscr{S}^{\mathrm{P}}$. For the sake of simplicity we have considered a single time level discretization.

Since we are considering situations where the coefficients (*i.e.* the fluid properties as density, viscosity) of the Navier-Stokes equations are certain, the operator $\mathcal{I}$ is deterministic and we have immediately

$$\left\langle \Psi_i \mathcal{I} \left(\sum_{j=0}^{\mathrm{P}} (\mathcal{U})_j^{n+1} \Psi_j \right) \right\rangle = \langle \Psi_i \Psi_i \rangle \, \mathcal{I} \, (\mathcal{U})_i^{n+1} . \tag{16}$$

In more general situations, the linear operator $\mathcal{I}$ depends on the random event, as for instance when the Reynolds number of the flow is random. In this case, one can formally expand the random operator $\mathcal{I}(\boldsymbol{\xi})$ on the stochastic basis:

$$\mathcal{I}(\boldsymbol{\xi}) = \sum_{i=0}^{\mathrm{P}} \mathcal{I}_i \Psi_i(\boldsymbol{\xi}). \tag{17}$$

As a result, application of $\mathcal{I}$ to $\mathcal{U}$ couples all the stochastic modes and Eq. (16) does not hold anymore. Instead, we have

$$\left\langle \Psi_i \mathcal{I} \left(\sum_{j=0}^{\mathrm{P}} (\mathcal{U})_j^{n+1} \Psi_j \right) \right\rangle = \sum_{j=0}^{\mathrm{P}} \sum_{l=0}^{\mathrm{P}} \langle \Psi_i \Psi_j \Psi_l \rangle \, \mathcal{I}_l \, (\mathcal{U})_j^{n+1} . \tag{18}$$

This coupling of the stochastic modes is not desirable as it significantly makes more difficult the inversion of $\mathcal{I}$. This difficulty can be easily overcome by using a semi implicit treatment of the linear terms, leading to a deterministic operator $\mathcal{I} \equiv \mathcal{I}_0$ and a modified operator $\mathcal{L}$ accounting for modes $\mathcal{I}_{i>0}$. An example of such a procedure to enforce a decoupled stochastic modes integration is provided in Section 6.

Assuming that Eq. (16) holds, and by making use of the orthogonality of the stochastic basis functions, Eq. (15) becomes

$$(\mathcal{U})_i^{n+1} = \mathcal{I}^{-1} \left\{ \mathcal{L}_i \left(\mathcal{U}^n \right) + \mathcal{N}_i \left(\mathcal{U}^n \right) + \mathcal{S}_i^{n+1} \right\}, \quad i = 0, 1, \ldots, \mathrm{P}. \tag{19}$$

This equation highlights the decoupling since the determination of $(\mathcal{U})_i^{n+1}$ is independent of $(\mathcal{U})_{j\neq i}^{n+1}$: the spectral problem has been factored in a series of $(\mathrm{P}+1)$ problems of smaller size. Comparison of Eq. (19) with Eq. (4) also reveals that the overall computational cost of the solution procedure will be $(\mathrm{P}+1)$ times greater than for the deterministic problem, with some additional overheads arising from the projection of the explicit terms $\mathcal{L}_i(\cdot)$, $\mathcal{S}_i(\cdot)$ and $\mathcal{N}_i(\cdot)$.

4. Resolution of steady stochastic equations

The decoupled resolution of the stochastic modes is an attractive feature of the solution method described above. However, one is often interested in finding solutions of the steady Navier-Stokes equation. Although the time integration of the unsteady equation may provide the steady solution as $t \to \infty$, they are many situations where computation of steady solution *via* unsteady integration is not desirable or practical: because of the slow decay of the unsteady solution toward a steady state (requiring integration over long periods of time) or because the sought steady solution is unstable to perturbations. In these cases the resolution of the steady equations has to be considered.

Direct determination of the solution to the steady equations is a difficult task, because of the size of the non-linear problem and of the non-trivial coupling between the stochastic modes. The question is therefore: how to take advantage of the decoupled time-marching schemes to compute stochastic solutions of the steady equations, even unstable ones ? This question has long been addressed in the deterministic context [35, 7], and we propose in the following an extension of these techniques to stochastic flows.

4.1. Newton iterations

It is clear that the determination of a (weak) solution of the steady stochastic Navier-Stokes equations consists in finding stationary points of Eq. (19) or, more specifically, to the determination of $\mathcal{U} \in \mathscr{V}_{\boldsymbol{u}_\Gamma} \otimes \mathscr{S}^{\mathrm{P}}$ such that

$$\frac{\partial \mathcal{U}}{\partial t} \approx \mathcal{F}(\mathcal{U}) \equiv \frac{\mathcal{I}^{-1}\left\{\mathcal{L}\left(\mathcal{U}\right) + \mathcal{S}\left(\boldsymbol{f}\right) + \mathcal{N}\left(\mathcal{U}\right)\right\} - \mathcal{U}}{\Delta t_n} = 0. \tag{20}$$

It is remarked that the "time-step" size is here denoted Δt_n, because it is a numerical parameter of the steady solver and not an actual time-step used to advance the solution in time. To solve Eq. (20), we rely on Newton iterations. Let $\mathcal{U}^k \in \mathscr{V}_{\boldsymbol{u}_\Gamma} \otimes \mathscr{S}^{\mathrm{P}}$ be the approximated solution of equation (20) after the k-the Newton iteration. The next Newton iterate, $\mathcal{U}^{k+1} \in \mathscr{V}_{\boldsymbol{u}_\Gamma} \otimes \mathscr{S}^{\mathrm{P}}$, is

$$\mathcal{U}^{k+1}(\boldsymbol{\xi}) = \mathcal{U}^k(\boldsymbol{\xi}) + \delta\mathcal{U}^k(\boldsymbol{\xi}), \tag{21}$$

where the stochastic Newton increment $\delta\mathcal{U}^k$ satisfies

$$\mathcal{J}(\mathcal{U}^k)\delta\mathcal{U}^k = -\mathcal{F}(\mathcal{U}^k). \tag{22}$$

Here, $\mathcal{J}(\mathcal{U})$ is the Jacobian of $\mathcal{F}$ at $\mathcal{U}$. Clearly, as $\mathcal{U}^k$ satisfies the boundary conditions, the Newton increment thus satisfies homogeneous Dirichlet velocity boundary conditions:

$$\delta\mathcal{U}^k \in \mathscr{V}_0 \otimes \mathscr{S}^{\mathrm{P}}. \tag{23}$$

The computation of $\mathcal{J}(\mathcal{U})$ is not an option because of its size, which is $(\mathrm{P}+1)$ times larger than its deterministic counterpart. However, it appears that $\mathcal{J}(\mathcal{U})\delta\mathcal{U}$ can be computed without making the Jacobian explicit as soon as one recognizes that

$$\mathcal{J}(\mathcal{U})\delta\mathcal{U} = \frac{\mathcal{I}^{-1}\left\{\mathcal{L}(\delta\mathcal{U}) + \overline{\mathcal{N}}\left(\mathcal{U}\right)\delta\mathcal{U}\right\} - \delta\mathcal{U}}{\Delta t_n}, \tag{24}$$

where $\overline{\mathcal{N}}(\mathcal{U})\delta\mathcal{U}$ are the non-linear terms linearized at $\mathcal{U}$. For the Navier-Stokes equations, the non-linearity comes from the convective terms. Although the actual forms of the convective terms depend on the selected formulation (*e.g.* on the variables in $\mathcal{U}$), we shall use the abusive notation $\mathcal{U}\boldsymbol{\nabla}\mathcal{U}$ for the convective terms. However, consistently with this notation, the linearized non-linear terms write as:

$$\overline{\mathcal{N}}\left(\mathcal{U}\right)\delta\mathcal{U} = -\mathcal{U}\boldsymbol{\nabla}\delta\mathcal{U} - \delta\mathcal{U}\boldsymbol{\nabla}\mathcal{U}. \tag{25}$$

In other words, $\mathcal{I}^{-1}\left\{\mathcal{L}\left(\delta\mathcal{U}\right) + \overline{\mathcal{N}}(\mathcal{U})\delta\mathcal{U}\right\}$ is the result of the time-integration (over a unique time-step) of the linearized stochastic Navier-Stokes equations, for the initial condition $\delta\mathcal{U} \in \mathscr{V}_0 \otimes \mathscr{S}^{\mathrm{P}}$ and homogeneous source term and velocity boundary conditions.

4.2. Stochastic increment problem

At this stage, we have derived an equation,

$$\frac{\mathcal{I}^{-1}\left\{\mathcal{L}(\delta\mathcal{U}^k) + \overline{\mathcal{N}}\left(\mathcal{U}^k\right)\delta\mathcal{U}^k\right\} - \delta\mathcal{U}^k}{\Delta t_n} + \mathcal{F}(\mathcal{U}^k) = 0, \tag{26}$$

for the stochastic Newton increment $\delta\mathcal{U}^k$. It remains to solve efficiently Eq. (26). To this end, consider the truncated expansions of the Newton iterates and increments:

$$\mathcal{U}^k(\boldsymbol{\xi}) = \sum_{i=0}^{\mathrm{P}} \left(\mathcal{U}^k\right)_i \Psi_i(\boldsymbol{\xi}), \quad \delta\mathcal{U}^k(\boldsymbol{\xi}) = \sum_{i=0}^{\mathrm{P}} \left(\delta\mathcal{U}^k\right)_i \Psi_i(\boldsymbol{\xi}). \tag{27}$$

The projection of Eq. (20) on the stochastic basis gives for $i = 0, \ldots, \mathrm{P}$:

$$\Delta t_n \mathcal{F}_i(\mathcal{U}^k) = \mathcal{I}^{-1}\left\{\mathcal{L}_i\left(\mathcal{U}^k\right) + \left(\mathcal{S}\right)_i + \mathcal{N}_i\left(\mathcal{U}^k\right)\right\} - \left(\mathcal{U}^k\right)_i. \tag{28}$$

The Galerkin projection of Eq. (24) gives in turn for $i = 0, \ldots, \mathrm{P}$:

$$\Delta t_n \left(\mathcal{J}(\mathcal{U}^k)\delta\mathcal{U}^k\right)_i = \mathcal{I}^{-1}\left\{\mathcal{L}_i\left(\delta\mathcal{U}^k\right) + \left(\overline{\mathcal{N}}\left(\mathcal{U}^k\right)\delta\mathcal{U}^k\right)_i\right\} - \left(\delta\mathcal{U}^k\right)_i, \tag{29}$$

Finally, equations to be solved for the Newton increment modes $\left(\delta\mathcal{U}\right)_l$ is for $i = 0, \ldots, \mathrm{P}$:

$$\mathcal{I}^{-1}\left\{\mathcal{L}_i\left(\delta\mathcal{U}^k\right) + \left(\overline{\mathcal{N}}\left(\mathcal{U}^k\right)\delta\mathcal{U}^k\right)_i\right\} - \left(\delta\mathcal{U}^k\right)_i = -\Delta t_n \mathcal{F}_i(\mathcal{U}^k). \tag{30}$$

It is seen that, although this equation is linear in the Newton increment, the determination of it stochastic modes $(\delta\mathcal{U})_i$ is coupled through the linearized non-linear term (except if $\mathcal{U}^k$ is actually deterministic). To gain further insight about this coupling, we make explicit the i-th mode of the linearized non-linear term. From Eq. (25), we have

$$\left(\overline{\mathcal{N}}(\mathcal{U})\delta\mathcal{U}\right)_i = -\frac{\langle(\mathcal{U}\boldsymbol{\nabla}\delta\mathcal{U} + \delta\mathcal{U}\boldsymbol{\nabla}\mathcal{U})\,\Psi_i\rangle}{\langle\Psi_i^2\rangle}, \tag{31}$$

and introducing the stochastic expansions of $\mathcal{U}$ and $\delta\mathcal{U}$, it comes

$$\begin{aligned}\left(\overline{\mathcal{N}}(\mathcal{U})\delta\mathcal{U}\right)_i &= -\sum_{j=0}^{\mathrm{P}}\sum_{l=0}^{\mathrm{P}} C_{ijl}\left((\mathcal{U})_j\boldsymbol{\nabla}(\delta\mathcal{U})_l + (\delta\mathcal{U})_j\boldsymbol{\nabla}(\mathcal{U})_l\right)\\ &= \sum_{j=0}^{\mathrm{P}}\sum_{l=0}^{\mathrm{P}} C_{ijl}\mathscr{C}\left[(\mathcal{U})_j, (\delta\mathcal{U})_l\right],\end{aligned} \tag{32}$$

where the bilinear convection operator $\mathscr{C}[.,.]$ and multiplication tensor C_{ijl} are defined by

$$\mathscr{C}[(\mathcal{U})_j, (\delta\mathcal{U})_l] \equiv (\mathcal{U})_j\boldsymbol{\nabla}(\delta\mathcal{U})_l + (\delta\mathcal{U})_l\boldsymbol{\nabla}(\mathcal{U})_j, \qquad C_{ijl} \equiv \frac{\langle\Psi_i\Psi_j\Psi_l\rangle}{\langle\Psi_i^2\rangle}. \tag{33}$$

With these notations, Eq. (30) can be rearranged to: for $i = 0, \ldots, \mathrm{P}$

$$\mathcal{I}^{-1}\left\{\mathcal{L}_i\left(\delta\mathcal{U}^k\right) + \sum_{j,l=0}^{\mathrm{P}} C_{ijl}\mathscr{C}\left[\left(\mathcal{U}^k\right)_j, \left(\delta\mathcal{U}^k\right)_l\right]\right\} - \left(\delta\mathcal{U}^k\right)_i = -\Delta t_n \mathcal{F}_i(\mathcal{U}^k). \tag{34}$$

It shows that it is not possible to decouple the problem for each mode $(\delta\mathcal{U})_i$.

4.3. Matrix free solver

We denote the linear operator $\mathcal{G} : (\mathcal{V},\mathcal{U}) \in (\mathscr{V}_0 \otimes \mathscr{S}^{\mathrm{P}}) \times (\mathscr{V}_{\boldsymbol{u}_\Gamma} \otimes \mathscr{S}^{\mathrm{P}}) \mapsto \mathcal{G}(\mathcal{V},\mathcal{U}) \in \mathscr{V}_0 \otimes \mathscr{S}^{\mathrm{P}}$ defined as

$$\mathcal{G}(\mathcal{V},\mathcal{U}) \equiv \mathcal{I}^{-1}\left\{\mathcal{L}\left(\mathcal{V}\right) + \overline{\mathcal{N}}\left(\mathcal{U}\right)\mathcal{V}\right\} - \mathcal{V}, \tag{35}$$

so one has to solve $\mathcal{G}(\mathcal{V},\mathcal{U}) = -\Delta t_n \mathcal{F}(\mathcal{U})$ for $\mathcal{V}$, given $\mathcal{U}$. As discussed previously, the first term in the expression of $\mathcal{G}$ in equation (35) is the result of a time integration of the linearized Navier-Stokes equations from the initial condition $\mathcal{V}$: a **decouple** time integration can be employed for its evaluation. This observation

suggests to use a matrix free method to solve Eq. (34) at the discrete level, *i.e.* after spatial discretization. Here, by matrix free method, we mean that the large system of algebraic equations corresponding to the discrete version of Eq. (34) is not constructed and inverted; this is essential due to the size of the discrete system, which we recall is (P + 1) times larger than in the deterministic context. Instead iterative techniques are considered for the determination of stochastic increment $\delta\mathcal{U}$, where for a given discrete iterate $\mathcal{V}$ the effect of the linear operator $\mathcal{G}(.,\mathcal{U})$ on $\mathcal{V}$ is obtained by means of a time-integration of the linearized Navier-Stokes equations. As a result, the computational cost to perform the pseudo matrix-vector product amounts to the resolution of one time step of the discrete unsteady linearized Navier-Stokes equation which, we emphasize, can be performed in a decoupled fashion. When selecting such matrix free iterative solver, it is important to recognize that the operator $\mathcal{G}$ is not self-adjoint. Two subspace methods for non-symmetric linear systems have been tested in this work for the resolution of the discrete version of Eq. (34): BiCGStab algorithm [31] and GMRES algorithm [29].

The efficiency of these algorithms is strongly related to the spectrum of $\mathcal{G}$, and the computational cost of the resolution mainly scales with the number of pseudo matrix-vector products (*i.e* integrations of the linearized discrete Navier-Stokes equations) needed to obtain the discrete increment within a given error tolerance. In fact, the overall computational cost to obtain the steady stochastic solution will depends on a) the convergence rate of the Newton iterations (which is independent of the iterative algorithm) and b) the number of integrations of the linearized Navier-Stokes equations to estimate the Newton increments (which depends on the iterative algorithm). It is expected that the convergence of the Newton iterations improves when Δt_n increases. In fact, Δt_n can be selected arbitrarily large, since no stability constraint holds. However, the choice of the time-step Δt_n also affects the spectrum of $\mathcal{G}$: using larger Δt_n will usually requires more integrations of the linearized Navier-Stokes equations to obtain the increment. Thus, we expect a trade-off on Δt_n, to balance the convergence of the Newton iterations with the numerical cost of computing the increments. This point is essential for the efficiency of the stochastic Newton solver and will be numerically illustrated in the next section.

Also related to the iterative algorithm used to compute the increments are memory requirements. The memory requirements are here a key aspect, as the size of the discrete solutions are (P + 1) times larger than for the deterministic problem. GMRES algorithm requires the storage of successive solution vectors to span the Krylov subspace. In contrast, BiCGStab algorithm needs to store of a fixed number (4) of solution vectors. Krylov subspaces of significant dimension are expected in order to approach the solution of Eq. (34) using GMRES. This makes the BiCGStab algorithm *a priori* more suited from memory requirements point of view. However, a comparison of the computational cost and memory requirements of the two methods is needed to decide which of the two algorithms should be preferred. This aspect is also investigated in the next section.

5. Test problem

5.1. Problem definition

The Newton method is tested on the normalized Boussinesq equations describing the natural convection flow inside a 2-dimensional square cavity: $(x, y) \in \Omega_x = [0, 1]^{d=2}$. The unsteady flow is governed by the the Boussinesq equations (Beqs), consisting in the momentum, energy and mass equations,

$$\left\{\begin{array}{l} \dfrac{\partial \boldsymbol{u}}{\partial t} + \boldsymbol{u}\cdot\boldsymbol{\nabla}\boldsymbol{u} = -\boldsymbol{\nabla}p + \dfrac{\mathrm{Pr}}{\sqrt{\mathrm{Ra}}}\nabla^2\boldsymbol{u} + \mathrm{Pr}T\boldsymbol{y}, \\ \dfrac{\partial T}{\partial t} + \boldsymbol{u}\cdot\boldsymbol{\nabla}T = \dfrac{1}{\sqrt{\mathrm{Ra}}}\nabla^2 T \\ \boldsymbol{\nabla}\cdot\boldsymbol{u} = 0, \end{array}\right. \tag{36}$$

where T is the normalized temperature, Ra is the Rayleigh number, Pr = 0.71 is the Prandtl number of the fluid (air) and $\boldsymbol{y}$ the gravity direction. Boundary conditions for the velocity are $\boldsymbol{u} = 0$ on Γ. For the temperature boundary conditions we assume adiabatic walls at $y = 0$ and 1 (top and bottom boundaries of

the cavity) and stochastic temperatures at $x = 0$ and 1 (vertical walls):

$$\begin{cases} \boldsymbol{\nabla} T \cdot \boldsymbol{y} = 0, & y = 0 \text{ and } 1, \\ T = T_\Gamma(\boldsymbol{\xi}), & x = 0 \text{ and } 1. \end{cases} \tag{37}$$

The linearized Boussinesq equations (LBeqs), around $(\boldsymbol{u}, T)$ satisfying the boundary conditions are

$$\begin{cases} \dfrac{\partial(\delta \boldsymbol{u})}{\partial t} + (\delta \boldsymbol{u}) \cdot \boldsymbol{\nabla} \boldsymbol{u} + \boldsymbol{u} \cdot \boldsymbol{\nabla}(\delta \boldsymbol{u}) = -\boldsymbol{\nabla}(\delta p) + \dfrac{\mathrm{Pr}}{\sqrt{\mathrm{Ra}}} \nabla^2(\delta \boldsymbol{u}) + \mathrm{Pr}(\delta T)\, \boldsymbol{y}, \\ \dfrac{\partial(\delta T)}{\partial t} + (\delta \boldsymbol{u}) \cdot \boldsymbol{\nabla} T + \boldsymbol{u} \cdot \boldsymbol{\nabla}(\delta T) = \dfrac{1}{\sqrt{\mathrm{Ra}}} \nabla^2(\delta T), \\ \boldsymbol{\nabla} \cdot (\delta \boldsymbol{u}) = 0, \end{cases} \tag{38}$$

with the homogeneous boundary conditions:

$$\begin{cases} \delta \boldsymbol{u} = 0, & \boldsymbol{x} \in \Gamma, \\ \boldsymbol{\nabla}(\delta T) \cdot \boldsymbol{y} = 0, & y = 0 \text{ and } 1, \\ \delta T = 0, & x = 0 \text{ and } 1. \end{cases} \tag{39}$$

These equations are solved in vorticity stream-function formulation (see [27]), on a uniform, staggered grid, using second order centered finite-differences schemes for the convective and viscous terms. Fast FFT-based solvers are used for the inversion of the heat and Poisson operators. Boundary conditions on the vorticity $\omega = (\boldsymbol{\nabla} \wedge \boldsymbol{u}) \cdot \boldsymbol{z}$ are determined through an influence matrix technique [5]. Using the formal notations, the solution of the Boussinesq equations is $\mathcal{U} = (\omega, T)$. For the purpose of the analysis, we define the stochastic norms $\| \cdot \|_{\Omega_x}^{\mathscr{S}^{\mathrm{P}}}$ by:

$$\left(\|f\|_{\Omega_x}^{\mathscr{S}^{\mathrm{P}}} \right)^2 \equiv \int_{\Omega_x} \left\langle f^2(x) \right\rangle dx = \sum_{i=0}^{\mathrm{P}} \left\langle \Psi_i^2 \right\rangle \int_{\Omega_x} (f(x))_i^2 \, d\boldsymbol{x}. \tag{40}$$

To monitor the convergence of the steady solution with the iterations, we use the norms of the steady vorticity and temperature equation residuals, denoted respectively $\|R_\omega\|_{\Omega_x}^{\mathscr{S}^{\mathrm{P}}}$ and $\|R_T\|_{\Omega_x}^{\mathscr{S}^{\mathrm{P}}}$, where using formal notations $R_\omega = \mathcal{F}_\omega(\mathcal{U})$ and $R_T = \mathcal{F}_T(\mathcal{U})$.

5.2. Unsteady simulations

In a preliminary test, the uncertain temperature boundary conditions is parameterized as follow:

$$\begin{cases} T_\Gamma(\xi) = \ \ 1/2 + 1/20\xi_1, & x = 0, \\ T_\Gamma(\xi) = -1/2 + 1/20\xi_2, & x = 1, \end{cases} \tag{41}$$

with ξ_1 and ξ_2 uniformly distributed on $[-1, 1]^2$. For these settings, the vertical walls support uniform independent random temperatures, with respective expectations equal to $\pm 1/2$, uncertainty levels $\pm 10\%$ and uniform probability densities. The stochastic dimension of the problem is then N = 2, and the orthogonal basis of $\mathscr{S}^{\mathrm{P}}$ is the set of 2-dimensional Legendre polynomials with degree less or equal to a prescribed expansion order No. The spectral problem is time-integrated from the initial conditions $\boldsymbol{u} = 0$, $T = 0$, using the decoupled strategy described in Section 3, with a first order backward Euler scheme with $\Delta t = 0.02$ on a 128×128 spatial grid.

In Figure 1, the convergence of the flow toward the steady state is monitored by plotting the steady residual norms $\|R_T\|_{\Omega_x}^{\mathscr{S}^{\mathrm{P}}}$ and $\|R_\omega\|_{\Omega_x}^{\mathscr{S}^{\mathrm{P}}}$ as functions of the time-iteration index. Different Rayleigh numbers are tested: $\mathrm{Ra} = 10^4$, 10^5 and 10^6. The expansion order is set to No = 3 in all the simulations, so $\dim(\mathscr{S}^{\mathrm{P}}) = 10$. The curves for the different Ra show a decay of the unsteady flow to their respective asymptotic stable steady states. However, the decay rate becomes slower as Ra increases, due to a weaker viscous damping of inertial waves. This behavior illustrates how the determination of a steady solution *via* time-integration, although possible in the range of Ra and temperature differences considered, becomes very inefficient when Ra increases.

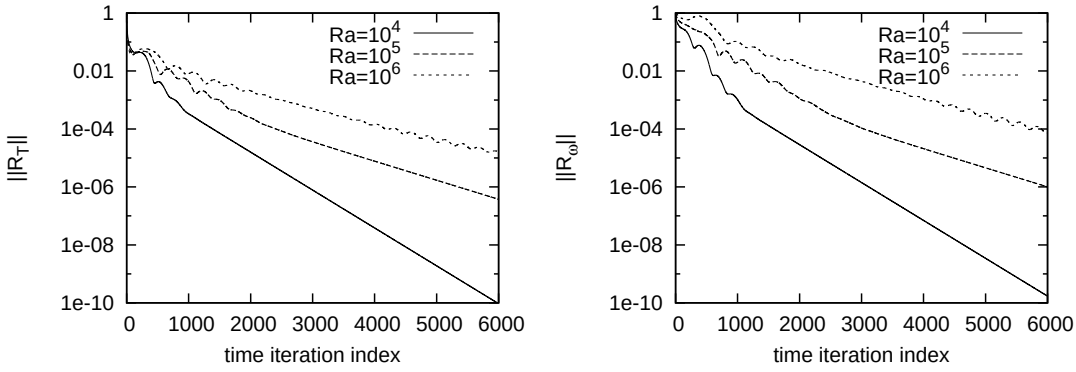

Figure 1: Decay with time-iterations of the steady residual norms $\|R_T\|_{\Omega_x}^{\mathscr{S}^{\mathrm{P}}}$ (left) and $\|R_\omega\|_{\Omega_x}^{\mathscr{S}^{\mathrm{P}}}$ (right) in unsteady simulations of the Boussinesq equations for $\mathrm{Ra} = 10^4$, 10^5 and 10^6 as indicated. The time-step is $\Delta t = 0.02$.

5.3. Newton iterations

The Newton iterations are now applied on the problem defined previously. The deterministic and stochastic discretizations are kept the same, except that $\Delta t_n = 5$ is now used. Newton iterations at a given Ra are initialized with the stochastic steady solution at Ra/2.

5.3.1. Convergence of Newton iterations

Figure 2 depicts the convergence with the Newton iterations of the steady residual norms $\|R_T\|_{\Omega_x}^{\mathscr{S}^{\mathrm{P}}}$ and $\|R_\omega\|_{\Omega_x}^{\mathscr{S}^{\mathrm{P}}}$. The computation of the Newton increments uses BiCGStab with a stopping criterion $\epsilon = 10^{-3}$ (see definition below). In these plots, the symbols correspond to the Newton iterates. For the three Ra tested, it is seen that 5 to 6 Newton iterations are needed to achieve a reduction of the residuals below 10^{-12}. The asymptotic convergence rate with the Newton iterations is found weakly dependent on Ra. However, the CPU costs dependent on Ra, as seen from the curves where the steady residual norms are reported as functions of the total number of LBeqs integrations performed. This trend denotes the degradation of the conditioning of the problem for the Newton increments when Ra increases. Specifically, it is seen that for $\mathrm{Ra} = 10^4$ about 10 iterations on the LBeqs are needed by BiCGStab to solve Eq. (22) within the requested tolerance, while ≈ 70 iterations are needed for the same tolerance criterion when $\mathrm{Ra} = 10^6$. However, keeping in mind that one iteration on the linearized equations (LBeqs) amounts essentially to the computational cost of one iteration of the unsteady equations (Beqs), the efficiency of the Newton method can be directly appreciated from a comparison of the decay rates of the residuals in Figures 2 and 1. For instance, when $\mathrm{Ra} = 10^6$ about 5000 unsteady iterations yield a reduction of the residual by a factor of roughly 10^3, to be compared with the reduction by a factor of roughly 10^{10} obtained in only 400 LBeqs iterations for the Newton method.

5.3.2. Stopping criterion

The Newton method being iterative, the increments $\delta\mathcal{U}^k(\boldsymbol{\xi})$ need not be exactly computed and approximated increments can be used instead, with the objective of reducing the CPU cost of their determination. In fact, iterations on the BiCGStab algorithm are performed as long as the probabilistic norms of the discrete equations $\mathcal{J}(\mathcal{U}^k)\delta\mathcal{U} = -\mathcal{F}(\mathcal{U}^k)$ (on T and ω), normalized by the norms of the respective right-hand sides, are such that

$$\frac{\|\mathcal{J}(\mathcal{U}^k)\delta\mathcal{U} + \mathcal{F}(\mathcal{U}^k)\|_{\Omega_x}^{\mathscr{S}^{\mathrm{P}}}}{\|\mathcal{F}(\mathcal{U}^k)\|_{\Omega_x}^{\mathscr{S}^{\mathrm{P}}}} > \epsilon, \tag{42}$$

for some small positive ϵ. In Figure 3, we compare the convergence of the steady residual norms at $\mathrm{Ra} = 10^6$ obtained using different ϵ in BiCGStab. It is seen that the residual reduction between two successive Newton iterates (symbols) improves when ϵ is lowered. However, this improvement becomes negligible when ϵ goes

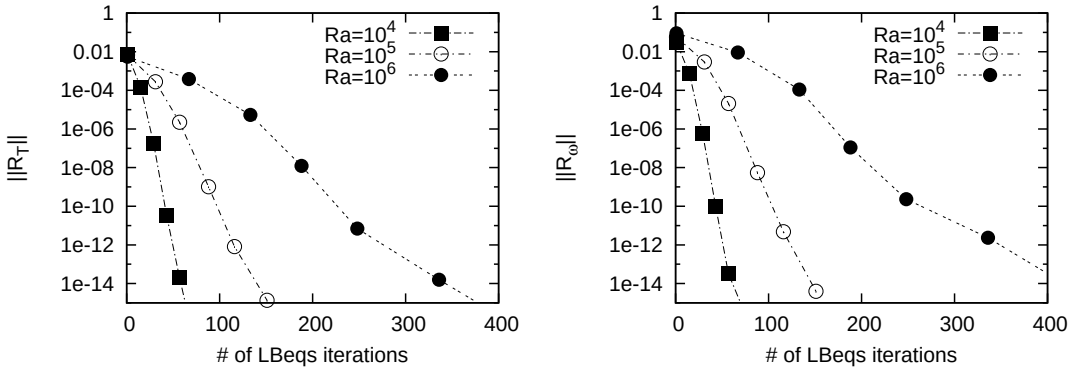

Figure 2: Convergence of the steady residual norms with the number of LBeqs iterations and for Ra $= 10^4$, 10^5 and 10^6 as indicated. Newton increments are computed using BiCGStab with $\Delta t_n = 5$ and stopping criterion $\epsilon = 10^{-3}$.

to zero and comes with a significant increase in the number of BiCGStab iterations. Therefore, there is a trade-off between the accuracy in the computed increment and the numerical cost of it resolution. For the present problem, the optimal trade-off in terms of number of LBeqs integrations is for $\epsilon \sim 10^{-1}, 10^{-2}$: for a similar reduction of the residuals, twice as many Newton iterations are needed than for $\epsilon = 10^{-4}$, but increments are obtained within 3 to 4 times less iterations.

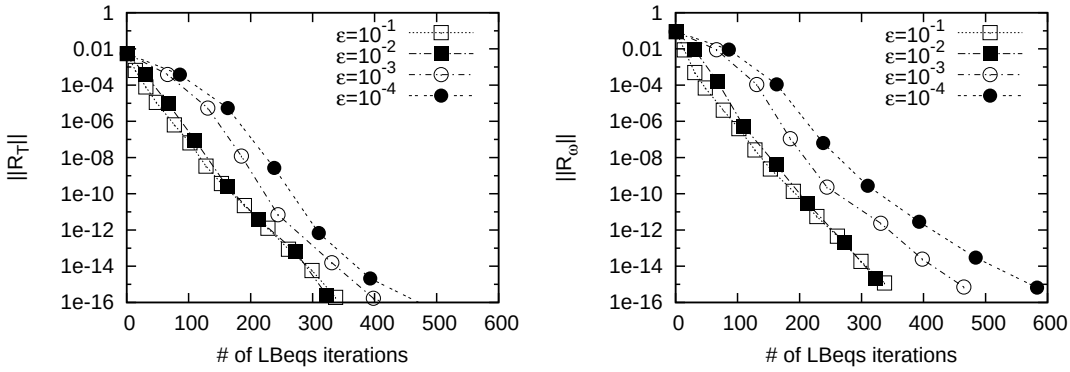

Figure 3: Convergence of the steady residual norms with the number of LBeqs iterations, for different stopping criteria ϵ as indicated and BiCGStab. Ra $= 10^6$, $\Delta t_N = 5$.

5.3.3. Newton time-step Δt_n

We recall that the selection of Δt_n is not subjected to stability restrictions and that the convergence of the Newton iterations is expected to improves when Δt_n increases. However, the conditioning of the problem on the increments is expected to degrade for increasing Δt_n, with a larger number of time integrations of the linearized problem as a result. These expectations are verified in the following tests for the solution at Ra $= 10^6$ using different time-steps and BiCGStab with $\epsilon = 10^{-3}$. The convergence of the steady residual norms is reported is Figure 4 and clearly evidences the expected trends: there is a optimal Δt_n balancing the steady residuals reduction, from a Newton iterate to the following, with the number of iterations needed to compute the increments. For the present test, $\Delta t_n \sim 5$ seems optimal in terms of number of iterations on the LBeqs. It has to be noticed that the *a priori* determination of the optimal Newton time-step, as well as the optimal stopping criterion, remains an open question. Furthermore, the respective CPU costs for the different values of Δt_n are here proportional to the number to LBeqs iterations, thanks to the use of FFT-based direct solvers for the diffusion and Poisson equations. In general, when using iterative solvers

for the integrations of the linearized equations such equivalence will not be true, and the comparison will have to be based on the actual CPU-times.

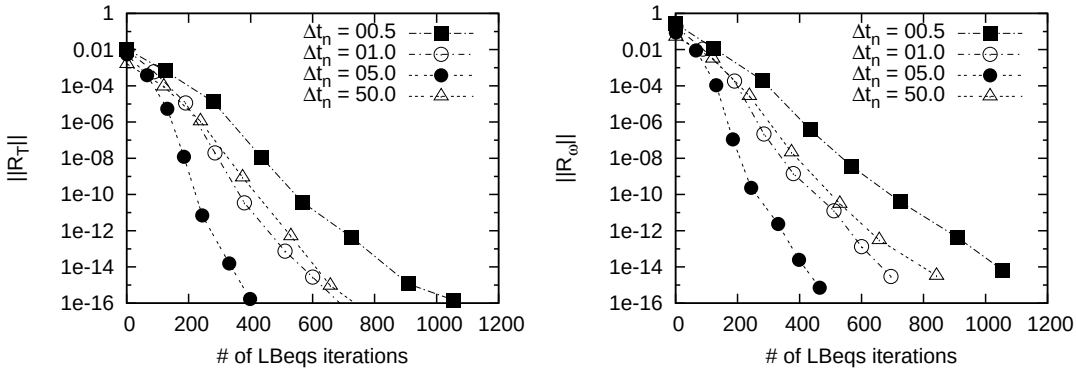

Figure 4: Convergence of steady residual norms with the number of LBeqs iterations using different Newton time-steps Δt_n as indicated. Ra $= 10^6$, BiCGStab algorithm with $\epsilon = 10^{-3}$.

5.3.4. GMRES vs BiCGStab

To complete this first series of tests, we provide a comparison of the respective efficiencies of BiCGStab and GMRES for the problem at Ra $= 10^6$. It is recalled that in addition to the CPU times, memory requirement is an important concern when designing solvers for stochastic spectral problems. Here, we take advantage of the relatively low dimensionality of the stochastic approximation space, $\dim(\mathscr{S}^{\mathrm{P}}) = 10$, to compare the respective efficiencies of the GMRES and BiCGStab algorithms. Indeed, for this problem we were able to construct Krylov subspaces sufficiently large to avoid the need of relying on restart procedures in GMRES.

Figure 5 compares the convergence of the steady residual norms using GMRES and BiCGStab, for two stopping criteria $\epsilon = 10^{-2}$ and $\epsilon = 10^{-4}$ and using $\Delta t_n = 5$. It is seen that for the two stopping criteria, GMRES requires less iterations than BiCGStab to approximate the Newton increments. Although significantly more efficient when $\epsilon = 10^{-4}$, one can observe that GMRES constructs Krylov subspaces with dimension up to 80, such that 80 solution vectors have to be stored, to be compared with only 4 in BiCGStab. Furthermore, the increments needing not to be accurately computed, as shown previously, BiCGStab is preferred and will be used systematically in the following.

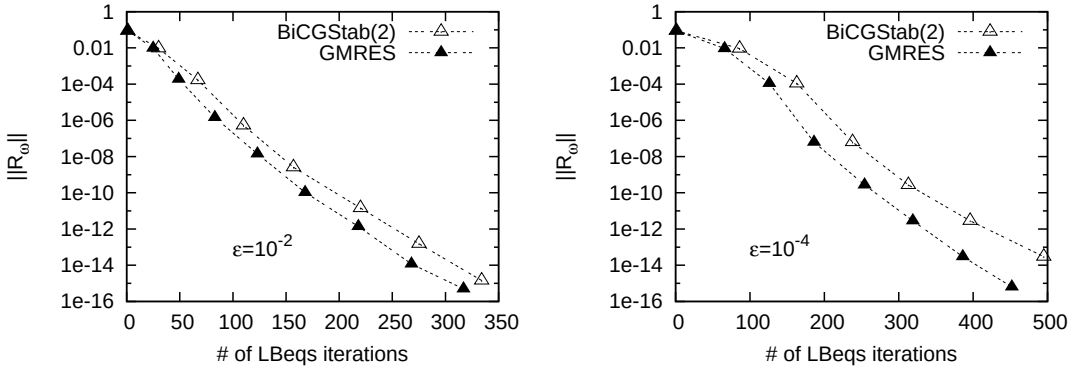

Figure 5: Comparison of convergences of the vorticity steady residual norm with the number of LBeqs iterations for BiCGStab (open symbols) and GMRES (filled symbols) algorithms and using different stopping criteria $\epsilon = 10^{-2}$ (left) and $\epsilon = 10^{-4}$ (right). Parameters are Ra $= 10^6$, $\Delta t_n = 5$.

5.4. Influence of the stochastic discretization

So far, we have verified that the behavior of the Newton method is consistent with our expectations based on theoretical analysis and our experience with deterministic problems. This was investigated by varying the parameters of the Newton method. This section aims at assessing the efficiency and robustness of the Newton method with regard to the stochastic discretization, *i.e.* when the stochastic approximation space $\mathscr{S}^{\mathrm{P}}$ changes.

To this end, we consider a more complex parameterization of the temperature boundary conditions. The temperature on the cold wall is now certain and equal to $T(x=1)=-1/2$, while the hot wall temperature is modeled as a stationary Gaussian stochastic process. This uncertainty setting corresponds to the problem treated in [22] which is now briefly summarized. The mean of the Gaussian stochastic process is $1/2$ with a standard deviation $\sigma_T = 0.1$: $T(x=0,y,\theta) \sim N(1/2, \sigma_T^2)$. The two points correlation function of the random temperature along the wall is assumed to decay exponentially with a characteristic length-scale $L=1$. The Karhunen-Loève (KL) expansion of the process is

$$T(x=0,y,\theta) = 1/2 + \sum_{k=1}^{\infty} \sqrt{\lambda_k} T_k(x=0,y)\xi_k(\theta), \tag{43}$$

where the normalized functions $T_k(x=0,y)$ are the deterministic KL modes and the ξ_k are uncorrelated (so independent) normalized centered Gaussian random variables:

$$\xi_k(\theta) \sim N(0,1), \quad \langle \xi_k \xi_l \rangle = \delta_{kl}. \tag{44}$$

Expressions for the deterministic KL modes can be found in [10, 22]. Ordering the KL modes of the temperature boundary conditions such that $\lambda_1 \geq \lambda_2 \geq \ldots$, the KL expansion is truncated after the N-th first terms. It comes

$$T(x=0,y,\theta) \quad \approx \quad T(x=0,y,\boldsymbol{\xi}(\theta)) = 1/2 + \sum_{k=1}^{\mathrm{N}} \sqrt{\lambda_k} T_k(x=0,y)\xi_k(\theta) \tag{45}$$

where $\boldsymbol{\xi} = \{\xi_1, \ldots, \xi_{\mathrm{N}}\}$. For the stochastic discretization, we rely on a Wiener-Hermite basis of $L^2(\Omega_{\boldsymbol{\xi}}, dP_{\boldsymbol{\xi}})$. Truncating the basis to order No yields the stochastic approximation space $\mathscr{S}^{\mathrm{P}}$, where P is given by Eq. (14). The expansions of the temperature and vorticity fields on the Wiener-Hermite basis are

$$T(x,y,\theta) = \sum_{k=0}^{\mathrm{P}} T_k(x,y)\Psi_k(\boldsymbol{\xi}), \quad \omega(x,y,\theta) = \sum_{k=0}^{\mathrm{P}} \omega_k(x,y)\Psi_k(\boldsymbol{\xi}). \tag{46}$$

The stochastic approximation space $\mathscr{S}^{\mathrm{P}}$ can be refined by increasing N and / or No. Our objective when selecting this problem was not to determine the minimal stochastic discretization to achieve given accuracy (this aspect was investigated in [22] where an unsteady integration was used), but rather to analyze the impact of the stochastic discretization on the efficiency of the Newton method.

5.4.1. Influence of the stochastic order No

In a series of simulations, we set $\mathrm{N}=4$, $\sigma_T = 0.1$ and we compute the steady solution for $\mathrm{Ra} = 10^6$ and different stochastic orders $\mathrm{No} = 1, \ldots, 5$. Each computation uses the corresponding steady solution for $\mathrm{Ra} = 5.10^5$ to initialize the Newton iterations. The increments are computed using BiCGStab with $\epsilon = 10^{-2}$ and $\Delta t_n = 5$. Figure 6 shows the convergence of the steady residuals for the different stochastic orders. It shows that the convergence rate of the Newton iterations is essentially independent of the expansion order No, as well as the the number of BiCGStab iterations needed to compute the increments.

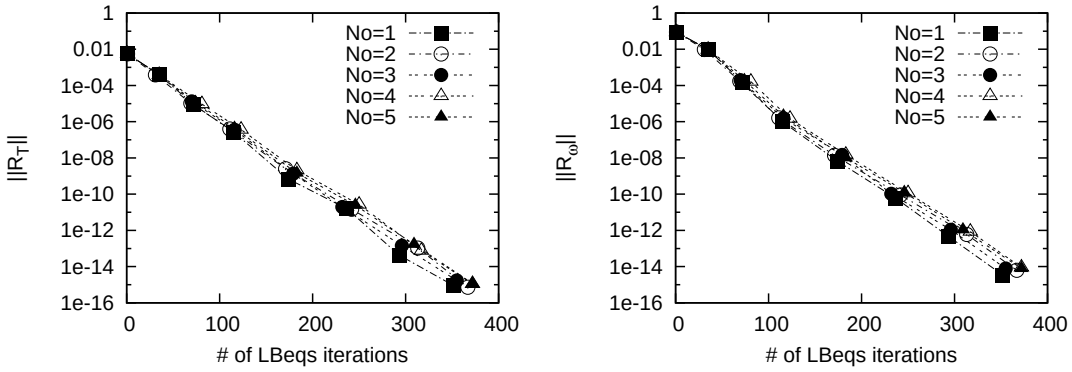

Figure 6: Convergence of the steady residual norms with the number of LBeqs iterations for different stochastic orders No = $1, \ldots, 5$. Computations use N = 4, BiCGStab with $\epsilon = 0.01$ and $\Delta t_n = 5$.

5.4.2. Influence of the stochastic dimension N

In a second series of tests, we fix the stochastic order to No = 3 and we increase the number of stochastic dimensions, *i.e.* the number of KL modes used to model the stochastic boundary conditions, from N = 3 to 8. Again, the Newton iterations are initialized with the respective steady solutions for Ra = 5.10^5, while BiCGStab is used with $\epsilon = 10^{-2}$ and $\Delta t_n = 5$. Inspection of the results reported in Figure 7 shows that the convergence of the Newton iterations, as well as the number of BiCGStab iterations for the increments computation, is essentially insensitive to the number N of stochastic dimensions.

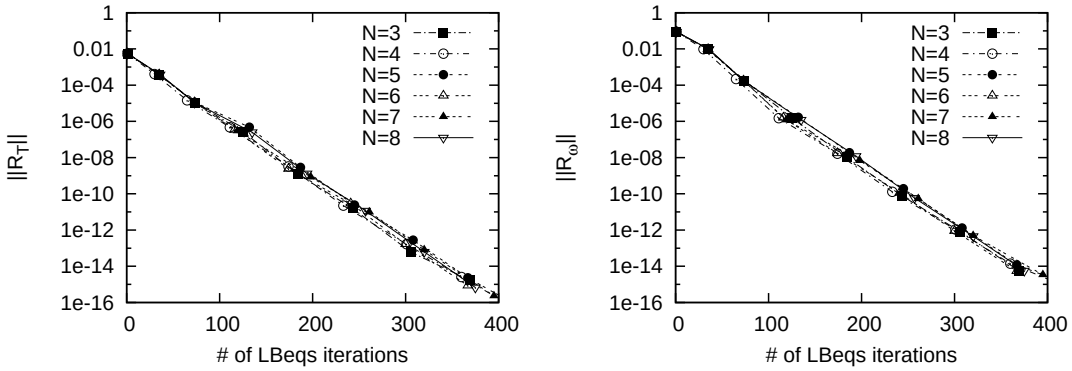

Figure 7: Convergence of the steady residual norms with the number of LBeqs iterations for different KL expansions of the temperature BCs with N = $3, \ldots, 8$. Computations use No = 3, BiCGStab with $\epsilon = 0.01$ and $\Delta t_n = 5$.

5.4.3. Comments

The two previous numerical experiments have shown a convergence of the Newton iterations essentially independent of the stochastic discretization. This is an interesting finding that was not necessarily expected. In fact, in view of Eq. (30) which exhibits the coupling between the spectral modes of the Newton increments, one may have anticipated an impact of the stochastic discretization on the number of BiCGStab iterations needed for the resolution of Eq. (22) as N and No increase. Such a trend is not reported in our simulations, denoting the robustness with regard to the stochastic discretization of the proposed method. In fact, the coupling between the stochastic modes in Eq. (22) is more related to the uncertainty level (or variability of the stochastic flow) than to the stochastic discretization. To support this claim, we consider the same problem and numerical parameters, but the standard deviation of the temperature boundary condition is double: $\sigma_T = 0.2$. Doubling the variability of the boundary condition increases the variability of the solution and so the magnitude of the stochastic modes and their non-linear interaction. In Figure 8, we compare

the convergence of the steady residuals in the simulations for $\sigma_T = 0.1$ and $\sigma_T = 0.2$ using No = 3 and N = 6. It is seen that the decay with the Newton iterations of the steady residuals is roughly unaffected when doubling σ_T, but that more BiCGStab iterations are needed to compute the increments.

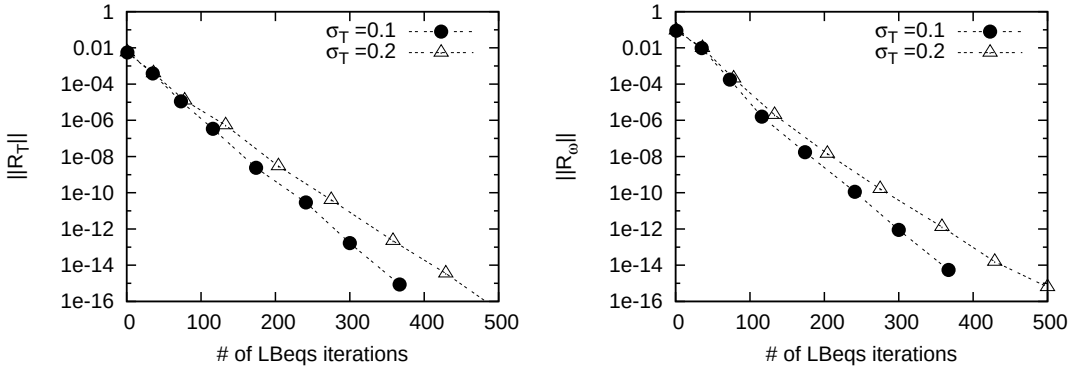

Figure 8: Convergence of the steady residual norms with the number of LBeqs iterations, for temperature BCs with standard deviation $\sigma_T = 0.1$ and 0.2. The stochastic discretization uses No = 3 and N = 6. Other parameters are given in the text.

5.5. Computational time

The independence with regard to the stochastic discretization of the residuals convergence, should not hide the fact that the computational cost significantly increases when the stochastic discretization is refined. We report in Table 1 the measured CPU-times of the simulations for $\sigma_T = 0.1$. All simulations were sequentially performed on a 64-bits bi-processor workstation (AMD Opteron 250, 2.4 GHz with 4Go of RAM). The variability in reported CPU-times is estimated to be ±10% (due to other running processes and time measurement errors). In addition to the CPU time, Table 1 also provides the corresponding dimensions of the stochastic approximation spaces, *i.e* the number of the stochastic modes in the solution. It is first remarked that for the largest stochastic space there are 165 stochastic modes, so the steady solution involves roughly 2.7 millions degrees of freedom and the steady solution is computed in slightly more than 2 hours of CPU.

N = 4	No = 1	No = 2	No = 3	No = 4	No = 5	
dim($\mathscr{S}^{\mathrm{P}}$)	5	15	35	70	126	
CPU times (s)	42	190	901	3,482	12,891	
No = 3	**N = 3**	**N = 4**	**N = 5**	**N = 6**	**N = 7**	**N = 8**
dim($\mathscr{S}^{\mathrm{P}}$)	20	35	56	84	120	165
CPU times (s)	373	901	1740	2,832	4,861	7,394

Table 1: CPU-times for the computation of the steady solutions at Ra = 10^6 using different expansion orders (No) and truncation (N) of the KL expansion for the temperature boundary condition.

To gain a better appreciation of the evolution of the CPU-time with the stochastic discretization, we have plotted in the left part of Figure 9 the measured CPU-times as a function of the dimensions (P + 1) of the stochastic approximation spaces. It is seen that for No = 3, the CPU-times scale asymptotically as dim($\mathscr{S}^{\mathrm{P}}$) when N increases. On the contrary, when N = 4 and No increases, a polynomial scaling of the CPU-time with dim($\mathscr{S}^{\mathrm{P}}$) is reported. These different scalings call for an explanation. It is first remarked that the total CPU-time is mostly spent in two distinct tasks. First, a large fraction of the CPU-time is spent solving the decoupled Poisson and diffusion operators for the stochastic solution modes: a scaling in $\mathcal{O}\dim(\mathscr{S}^{\mathrm{P}})$ for this contribution to the CPU-time is expected. The second time-consuming part of the

computation comes with the projection of the explicit terms. For the LBeqs, the cost for the projection of the explicit terms is dominated by the stochastic products, which scale with the complexity $\mathcal{C}$ of the Galerkin product. This complexity can be measured [20] as the number of non zero entries in the multiplication tensor $C_{klm} = \langle \Psi_k \Psi_l \Psi_m \rangle / \langle \Psi_k^2 \rangle$. The complexity $\mathcal{C}$ is a function of both No and N. With these notations, the total CPU-time scales as $\mathcal{O}\dim(\mathscr{S}^{\mathrm{P}}) + \mathcal{O}(\mathcal{C}(\mathrm{N}, \mathrm{No}))$. The right plot in Figure 9 shows $\mathcal{C}$ for the stochastic discretizations tested. It is seen that for fixed expansion order (No = 3) the scaling of $\mathcal{C}$ with $\dim(\mathscr{S}^{\mathrm{P}})$ is asymptotically linear, while for a fixed number of stochastic dimensions (N = 4) the scaling is polynomial in $\dim(\mathscr{S}^{P})$ as No increases. These two trends explain the reported evolutions of the total CPU-time with the stochastic discretization: for fixed expansion order the CPU-time is essentially proportional to the stochastic basis dimension, while for fixed N the contribution of the explicit terms projection to the CPU-time becomes more and more important as No increases.

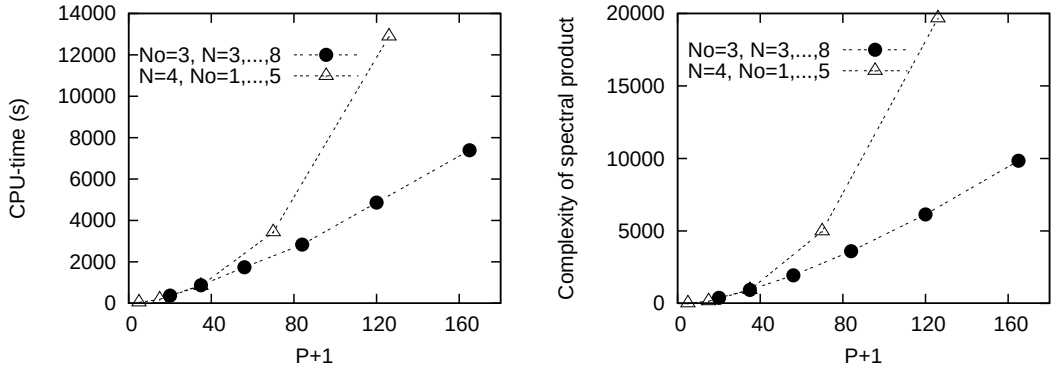

Figure 9: CPU-times for the resolution of the steady problem (left) and complexity $\mathcal{C}$ of the Galerkin product (right) for different stochastic discretizations.

6. Unstable steady flow

In this section, we provide a last example for the application of the Newton method. The objective of this example is two folds. First, it aims at demonstrating the effectiveness of the proposed method when dealing with steady flows likely unstable to perturbations. Second, the example is used illustrate the decoupling strategy mentioned in Section 3.3.

6.1. Uncertainty settings

We consider the normalized two-dimensional flow around a circular cylinder. The flow is characterized by the Reynolds number $\mathrm{Re} = U_\infty D/\nu$, where U_∞ is the free-stream velocity, D the cylinder diameter and ν the fluid viscosity. It is well known that this flow is unstable for $\mathrm{Re} > 48$. We assume deterministic free-stream velocity and cylinder diameter, and consider a uncertainty in the fluid viscosity ν, modeled as a Log-Normal random variable with median value $\overline{\nu}$ and coefficient of variation $a > 1$; *i.e.* ν is expected to be in the range $[\overline{\nu}/a, \overline{\nu}a]$ with 99% probability. The random viscosity can be parameterized using a unique random variable ξ as follow:

$$\nu(\xi) = \exp(-\mu + \sigma\xi), \quad \mu = \log \overline{\nu}, \quad \sigma = \log(a)/2.95. \tag{47}$$

The stochastic basis consists in one-dimensional Hermite polynomials. On this basis, ν has for stochastic expansion:

$$\nu(\xi) = \sum_i \nu_i \Psi_i(\xi) = \exp(\mu + \sigma^2/2) \sum_i \frac{\sigma^i}{\langle \Psi_i^2 \rangle} \Psi_i(\xi), \tag{48}$$

where Ψ_i is the Hermite polynomial with degree i. The median value of the viscosity is set such that the median Reynolds number $\overline{\mathrm{Re}} = U_\infty D/\overline{\nu} = 60$ and the coefficient of variation is fixed to $a = 3/2$. Therefore,

most realizations of the stochastic flow are above the critical Reynolds number as one can appreciate from Figure 10 which depicts the probability density function of Re.

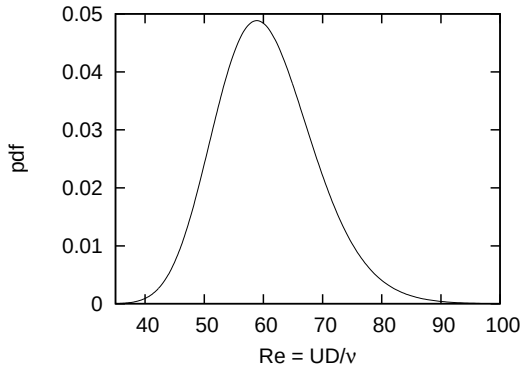

Figure 10: Probability density function of the stochastic Reynolds number of the flow.

6.2. Flow equations and stochastic decoupling

The vorticity stream-function formulation of the flow is considered in an annular domain extending from the cylinder boundary Γ_c to an external circular boundary Γ_∞ located at $25D$ from the cylinder center. The governing equations of the flow are

$$\begin{cases} \dfrac{\partial \omega}{\partial t} = -\boldsymbol{u}\cdot\boldsymbol{\nabla}\omega + \dfrac{1}{\mathrm{Re}}\nabla^2\omega, \\ \nabla^2\psi = -\omega, \\ \boldsymbol{u} = \boldsymbol{\nabla}\wedge(\psi\boldsymbol{k}), \end{cases} \tag{49}$$

where ω is the vorticity and ψ the stream-function. Natural boundary conditions are $\boldsymbol{u} = 0$ on Γ_c and $\boldsymbol{u} = U_\infty \boldsymbol{i}$ on Γ_∞. The flow variables are expanded on the Hermite basis and introduced in the Eq. (49) which are in turn projected on the spectral basis. For a truncation of the stochastic basis to stochastic order No, it led for $i = 0, \ldots, \mathrm{P} = \mathrm{No}$,

$$\begin{cases} \dfrac{\partial(\omega)_i}{\partial t} = -\displaystyle\sum_j \sum_l C_{ijl}\left[(\boldsymbol{u})_j \boldsymbol{\nabla}(\omega)_l + \left(\frac{1}{\mathrm{Re}}\right)_j \nabla^2(\omega)_l\right], \\ \nabla^2(\psi)_i = -(\omega)_i, \\ (\boldsymbol{u})_i = \boldsymbol{\nabla}\wedge((\psi)_i\boldsymbol{k}). \end{cases} \tag{50}$$

The next step is to select a time-discretization that decouples the integration of the stochastic modes. This is achieved by splitting the stochastic diffusion term as follow:

$$\begin{aligned} \sum_j \sum_l C_{ijl}\left(\frac{1}{\mathrm{Re}}\right)_j \nabla^2(\omega)_l &= \sum_l C_{i0l}\left(\frac{1}{\mathrm{Re}}\right)_0 \nabla^2(\omega)_l \\ &+ \sum_{j>0}\sum_l C_{ijl}\left(\frac{1}{\mathrm{Re}}\right)_j \nabla^2(\omega)_l, \\ &= \left(\frac{1}{\mathrm{Re}}\right)_0 \nabla^2(\omega)_i + \sum_{j>0}\sum_l C_{ijl}\left(\frac{1}{\mathrm{Re}}\right)_j \nabla^2(\omega)_l. \end{aligned} \tag{51}$$

In the previous equation, we have assumed an indexation of the polynomials Ψ_i in the stochastic basis with increasing degree, such that Ψ_0 is the zero degree (constant) polynomial; we set $\Psi_0 = 1$. With this

classical indexation $C_{i0l} = \delta_{il}$. Introducing a first order time discretization, the semi-discrete equation for the vorticity mode $(\omega)_i$ is

$$\left(\frac{1}{\Delta t} - \left(\frac{1}{\mathrm{Re}}\right)_0 \nabla^2\right)(\omega^{n+1})_i = \frac{(\omega^n)_i}{\Delta t} + \sum_{j>0}\sum_l C_{ijl}\left(\frac{1}{\mathrm{Re}}\right)_j \nabla^2(\omega^n)_l - \sum_j\sum_l C_{ijl}\,(\boldsymbol{u}^n)_j\,\boldsymbol{\nabla}\,(\omega^n)_l\,, \tag{52}$$

or using the formal notations

$$\mathcal{I}\,(\omega)_i^{n+1} = \mathcal{L}_i\,(\omega^n) + \mathcal{N}_i(\omega^n). \tag{53}$$

The annular domain is conformally mapped to a rectangular mathematical domain where the equations are solved. On the opposite sides of the mathematical domain corresponding to Γ_c and Γ_∞, boundary conditions for the vorticity modes $(\omega)_i$ are determined by means of an influence matrix technique [5, 30, 37, 23]. The spatial discretization uses second order centered finite-differences schemes on a uniform grid with 256×512 points, allowing for fast FFT-based solvers for the inversion of the Poisson and diffusion operators. The Hermite expansion is truncated at $\mathrm{No} = 4$ so they are $\mathrm{P} + 1 = 5$ modes in the solution.

6.3. Results

We apply the Newton method to solve the steady stochastic flow, with $\Delta t_n = 10$ and $\epsilon = 0.01$ in BiCGStab algorithm. Newton iterations are initialized with $\omega^0(\xi) = 0$. For this initialization a limiter on the Newton increments is needed. This limiter rescales the increment by a small positive constant when the norm $\|\delta\mathcal{U}\|^{\mathscr{I}^{\mathrm{P}}}_{\Omega_x}$ is deemed too large. In the computation presented, the limiter acts only during the first three Newton iterations. Figure 11 presents the convergence of the steady residual with the Newton iterations. It is interesting to note that the number of BiCGStab iterations needed to satisfy the stopping criterion increases with the Newton index (not shown). This can be explained by the degradation of the conditioning of the increment problem, as the stochastic modes develop. A total of 1,175 linearized time-integrations was necessary to obtain a residual below 10^{-14}.

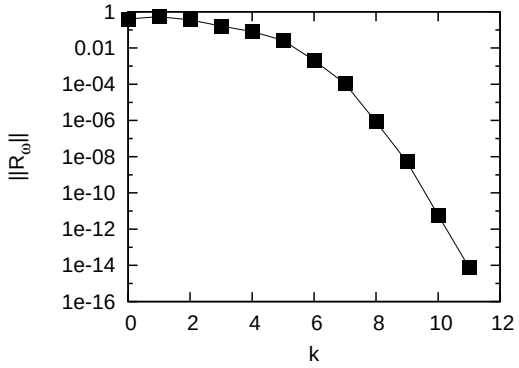

Figure 11: Convergence of the steady equation residual as a function of the Newton iteration index k.

Figure 12 presents the evolution during the first five Newton iterations of the averaged flow, *i.e.* the mode $i = 0$ of the solution. Plotted are the streamlines (top part of the plots) and vorticity contours (bottom part of the plots) for the flow going from left to right. It shows the development of the two symmetric recirculation zones and the convection in the downstream direction of the vorticity.

Figure 13 presents the stochastic modes of the stream-function $(\psi)_i$ (top part of the plots) and vorticity field $(\omega)_i$ (bottom part of the plots) of the steady solution, for modes $i = 0, \ldots, 3$. The contours level have been adapted in each plot to highlight the flow structure, but it is underlined that the magnitude of the fields decays by a factor of 50 to 100 between two successive modes (denoting the convergence of the stochastic expansion). The plots show that the uncertainty in the fluid viscosity essentially affects the vorticity field

in the boundary layers and in the cylinder wake. On the contrary, the stream-function modes denote an impact of the uncertainty which extends far from the cylinder, even-though it primary affects the magnitude and spatial extension of the recirculation zones behind the cylinder.

To gain a better appreciation of the steady flow variability with regard to the uncertain viscosity, we present in Figure 14 the standard deviation fields of the stochastic vorticity, stream-function and velocity components. The standard deviation of the vorticity field confirms that the uncertainty essentially affects the vorticity in the boundary layers and cylinder wake. The standard deviation of the stream-function highlights the variability in the intensity and spatial extension of the symmetric recirculation downstream of the cylinder. The standard deviation of the velocity component u, parallel to the inflow velocity, shows that it is mostly affected by the uncertainty along the flow symmetry axis and in the recirculation zones. On the contrary of u, the transverse fluid velocity v exhibits a maximum variability in the immediate neighborhood of the up-stream boundary layers, and is null on the axis of symmetry, since all realizations of the flow are symmetric.

Finally, Figure 15 shows in the top plot the resulting viscous stress distribution over the cylinder boundary, using the classical representation with mean value and uncertainty bounds extending to ± 3 standard deviations. The bottom plot of Figure 15 provides an analysis of the flow recirculation statistics. Specifically, it shows as a function of the downstream distance x/D from the cylinder center, the longitudinal velocity u (mean value and ± 3 standard deviations bounds), the probability of u to be negative (*i.e.* the probability of point x/D to be in the recirculation zone) and the probability density (rescaled by its maximum) of having $u(x/D) = 0$ (*i.e.* the probability density that the recirculation extends up to x/D).

7. Conclusion and summary

A Newton method has been proposed for the resolution of the stochastic incompressible steady Navier-Stokes equations. The method is an extension of the technique developed in the deterministic context. It relies on an appropriate time discretization of the unsteady equations to derive a convenient stochastic spectral problem for the Newton increments of the steady solution. The method leads to matrix-free strategies, where the Newton increments are iteratively computed by solving a series of spectral problems consisting in the time integration (over one pseudo time-step) of the linearized unsteady stochastic flow equations. The procedure offers several advantages:

1. it avoids the explicit construction of the large equations Jacobian,
2. the adaptation of an unsteady stochastic flow solver to the resolution of the linearized problem is generally straightforward,
3. the time integration of the spectral modes is decoupled.

Numerical experiments and examples provided in the result sections have demonstrated the efficiency of the method. Major findings are summarized as follow:

- A fast converge of the Newton iterations is reported in all the simulations, even for flows unstable to perturbations.
- The convergence rate of the Newton iterations is essentially independent of the stochastic discretization.
- The number of iterations on the linearized unsteady problem is also essentially independent of the stochastic discretization, although it increases with the flow variability.
- Newton increments can be roughly computed, thus reducing the number of integrations of the unsteady linearized problem to be performed.
- The efficiency of the method depends on the selected pseudo time-step. There is an optimal time-step, but we are not able to determine it value *a priori*.
- For the computation of the Newton-increments, we recommend to use BiCGStab: although slightly less efficient than GMRES on the tested problems, it has much lower memory requirements.

- The analysis of the CPU-times have shown that for large stochastic approximation spaces, the computational times tend to scale with the complexity (number of operations) in the spectral product. This scaling denotes the increasing proportion of the time spent for the projection of the explicit terms to the overall CPU-times when the order of the stochastic discretization is refined.

Following these findings, future improvement(s) should focus on the optimization of the Newton increments computation. Specifically, these increments being the solution of a linear problem, the so-called Generalized Spectral Decomposition recently proposed in [26] is an attractive strategy that is expected to drastically reduce both CPU-times and memory requirements for their approximation. This is the focus of an on-going work.

References

[1] M. Abramowitz and I.A. Stegun. *Handbook of Mathematical Functions*. Dover, 1970.

[2] I. Babuska and P. Chatzipantelidis. On solving elliptic stochastic partial differential equations. *Comput. Methods Appl. Mech. and Engrg.*, 191:4093–4122, 2002.

[3] R.H. Cameron and W.T. Martin. The orthogonal development of nonlinear functionals in series of Fourier-Hermite functionals. *Ann. Math.*, 48:385–392, 1947.

[4] A.J. Chorin. A numerical method for solving incompressible viscous flow problems. *J. Comput. Phys.*, 2:12–26, 1967.

[5] O. Daube. An influence matrix technique for the resolution of 2d Navier-Stokes equation in velocity-vorticity formulation. In *Int. Conf. Num. Meth. in Laminar and Turbulent Flows*, 1986.

[6] B. Debusschere, H.N. Najm, A. Matta, O.M. Knio, R.G. Ghanem, and O.P. Le Maître. Protein labeling reactions in electrochemical microchannel flow: Numerical prediction and uncertainty propagation. *Physics of Fluids*, 15(8):2238–2250, 2003.

[7] W.S. Edwards, L.S. Tuckerman, R.A. Friesner, and D.C. Sorensen. Krylov methods for the incompressible navier-stokes equations. *J. Comput. Physics*, 110(1):82–102, 1994.

[8] R. Ghanem and S. Dham. Stochastic finite element analysis for multiphase flow in heterogeneous porous media. *Transp. Porous Media*, 32:239–262, 1998.

[9] R.G. Ghanem. Probabilistic characterization of transport in heterogeneous media. *Comp. Meth. App. Mech. Eng.*, 158:199–220, 1998.

[10] R.G. Ghanem and P.D. Spanos. *Stochastic Finite Elements: A Spectral Approach*. Dover, 2002. 2nd edition.

[11] T.D. Hien and M. Kleiber. Stochastic finite element modeling in linear transcient heat transfer. *Comp. Met. App. Mech. Eng.*, 144:111–124, 1997.

[12] M. Kaminski and T.D. Hien. Stochastic finite element modeling of transcient heat transfer in layered composites. *International Communication in Heat and Mass Transfer*, 26(6):801–810, 1999.

[13] J. Kim and P. Moin. Application of a fractional-step method to incompressible navier-stokes equations. *J. Comput. Phys.*, 59:308–323, 1985.

[14] O.M. Knio and O.P. Le Maître. Uncertainty propagation in cfd using polynomial chaos decomposition. *Fluid Dyn. Res.*, 38:616–640, 2006.

[15] O. Le Maître, O.M. Knio, B. Debusschere, H.N. Najm, and R.G. Ghanem. A multigrid solver for two-dimensional stochastic diffusion equations. *Comput. Methods App. Mech. Engrg.*, 192(41-42):4723–4744, 2003.

[16] O. Le Maître, M.T. Reagan, B. Debusschere, H.N. Najm, R.G. Ghanem, and O.M. Knio. Natural convection in a closed cavity under stochastic, non-Boussinesq conditions. *J. Sci. Comput.*, 26(2):375–394, 2004.

[17] O.P. Le Maître and O.M. Knio. A stochastic particle-mesh scheme for uncertainty propagation in vortical flows. *J. Comput. Phyics*, 226:645–671, 2007.

[18] O.P. Le Maître, O.M. Knio, H.N. Najm, and R.G. Ghanem. A stochastic projection method for fluid flow. i. basic formulation. *J. Comput. Phyics*, 173:481–511, 2001.

[19] O.P. Le Maître, O.M. Knio, H.N. Najm, and R.G. Ghanem. Uncertainty propagation using Wiener-Haar expansions. *J. Comput. Phyics*, 197(1):28–57, 2004.

[20] O.P. Le Maître, H.N. Najm, R.G. Ghanem, and O.M. Knio. Multi-resolution analysis of Wiener-type uncertainty propagation schemes. *J. Comput. Physics*, 197(2):502–531, 2004.

[21] O.P. Le Maître, H.N. Najm, P.P. Pébay, R.G. Ghanem, and O.M. Knio. Multi-resolution-analysis scheme for uncertainty quantification in chemical systems. *SIAM J. Sci. Comput.*, 29(2):864–889, 2007. in press.

[22] O.P. Le Maître, M.T. Reagan, H.N. Najm, R.G. Ghanem, and O.M. Knio. A stochastic projection method for fluid flow. ii. random process. *J. Comput. Phyics*, 181:9–44, 2002.

[23] O.P. Le Maître, R.H. Scanlan, and O.M. Knio. Numerical estimation of the flutter derivatives of a NACA airfoil by means of Navier-Stokes simulation. *J. Fluids and Structures*, 17(1):1–28, 2003.

[24] N. Liu, B. Hu, and Z.-W. Yu. Stochastic finite element method for random temperature in concrete structures. *International Journal of Solids and Structures*, 38:6965–6983, 2001.

[25] H. G. Matthies and A. Keese. Galerkin methods for linear and nonlinear elliptic stochastic partial differential equations. *Computer Methods in Applied Mechanics and Engineering*, 194(12-16):1295–1331, 2005.

[26] A. Nouy. A generalized spectral decomposition technique to solve a class of linear stochastic partial differential equations. *Computer Methods in Applied Methods in Engineering*, 196(45-48):4521–4537, 2007.

[27] R. Peyret. *Spectral Methods for Incompressible Viscous Flow*. Number 148 in Applied Mathematical Sciences. Springer-Verlag, 2002.
[28] M.T. Reagan, H.N. Najm, B.J. Debusschere, O.P. Le Maître, O.M. Knio, and R.G. Ghanem. Spectral stochastic uncertainty quantification in chemical systems. *Combustion Theory and Modelling*, 8:607–632, 2004.
[29] Y. Saad and M.H. Schultz. GMRES: a generalized minimal residual algorithm for solving nonsymmetric linear system. *J. Sci. Stat. Comput.*, 7:856–869, 1986.
[30] W.-Z. Shen and T.-P. Loc. Simulation of 2d external viscous flow by means of a domain decomposition method using an influence matrix technique. *Int. J. Numer. Meth. Fluids*, 20:1111, 1995.
[31] G.L.G. Sleijpen and D.R. Fokkema. BICGSTAB(L) for linear equations involving unsymmetric matrices with complex spectrum. *ETNA*, 1:11–32, 1993.
[32] C. Soize. A comprehensive overview of a non-parametric probabilistic approach of model uncertainty for predictive models in structural dynamics. *J. Sound and Vibrations*, 288:623–652, 2005.
[33] C. Soize. Random matrix theory for modeling uncertainty in computational mechanics. *Comput. Methods App. Mech. and Engrg.*, 194(12-16):1333–1366, 2005.
[34] C. Soize and R. Ghanem. Physical systems with random uncertainties : chaos representations with arbitrary probability measure. *J. Sci. Comput.*, 26(2):395–410, 2004.
[35] L.S. Tuckerman. Steady-state solving via stokes preconditioning; recursion relations of elliptic operators. In *11-th Int. Conf. on Numer. Meth. in Fluid Dynamics*. Springer-Verlag, 1989.
[36] L.S. Tuckerman, C. Huepe, and M.-E. Brachet. Numerical methods for bifurcation problems. In O. Descalzi, J. Martinez, and S. Rica, editors, *Instabilities and non-equilibrium structures IX*. Kluwer, 2004.
[37] J.M. Vanel, R. Peyret, and P. Bontoux. A pseudo-spectral solution of vorticity-stream-function equations using the influence matrix technique. *Num Meth Fluid Dyn II*, pages 463–475, 1986.
[38] X. Wan and G.E. Karniadakis. An adaptative multi-element generalized polynomial chaos method for stochastic differential equations. *J. Comput. Physics*, 209:617–642, 2005.
[39] S. Wiener. The Homogeneous Chaos. *Amer. J. Math.*, 60:897–936, 1938.
[40] D.B. Xiu and G.E. Karniadakis. The Wiener-Askey Polynomial Chaos for stochastic differential equations. *SIAM J. Sci. Comput.*, 24:619–644, 2002.
[41] D.B. Xiu and G.E. Karniadakis. Modeling uncertainty in flow simulations via generalized Polynomial Chaos. *J. Comput. Physics*, 187:137–167, 2003.

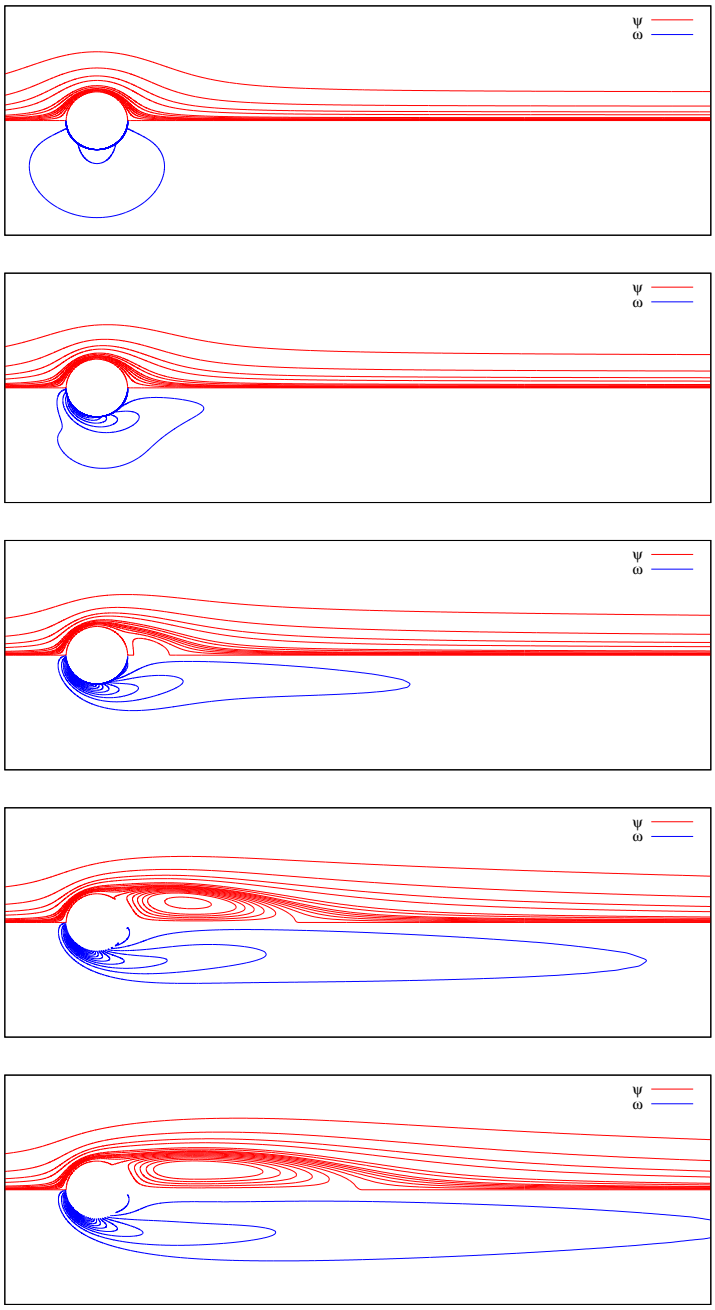

Figure 12: Evolution with the first Newton iterates ($k = 1, \ldots, 5$ from top to bottom) of the averaged flow streamlines (top part of the plots) and vorticity contours (bottom part of the plots). The flow is from left to right.

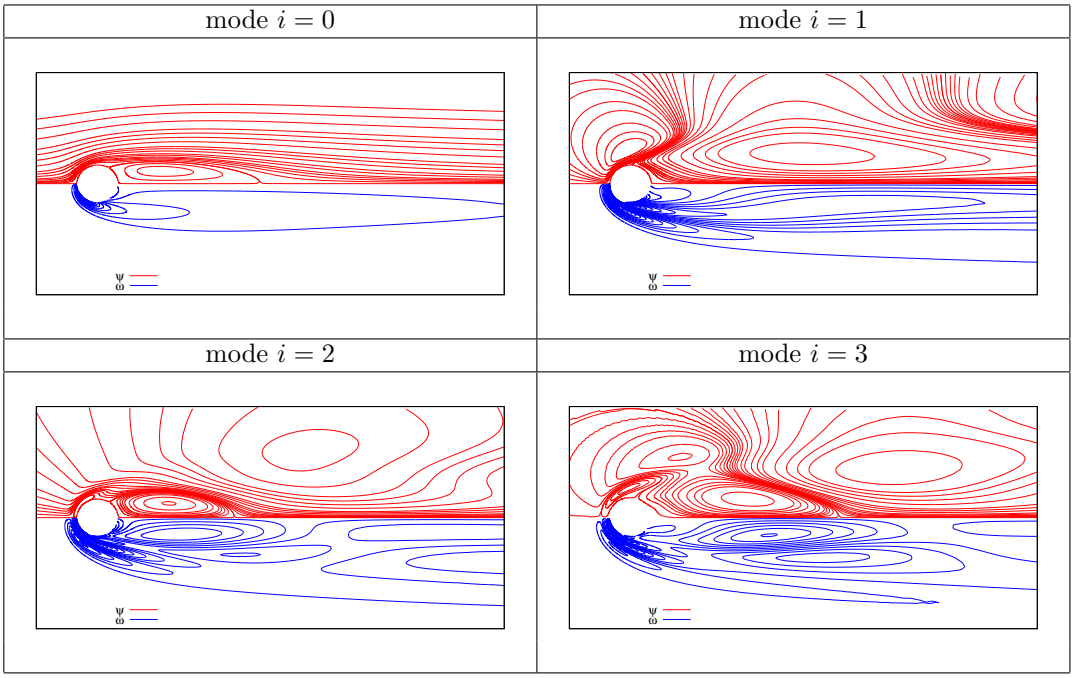

Figure 13: Stochastic modes $i = 0, \ldots, 3$ of the steady stream-function $(\psi)_i$ (top part of the plots) and vorticity field $(\omega)_i$ (bottom part of the plots). The flow goes from left to right.

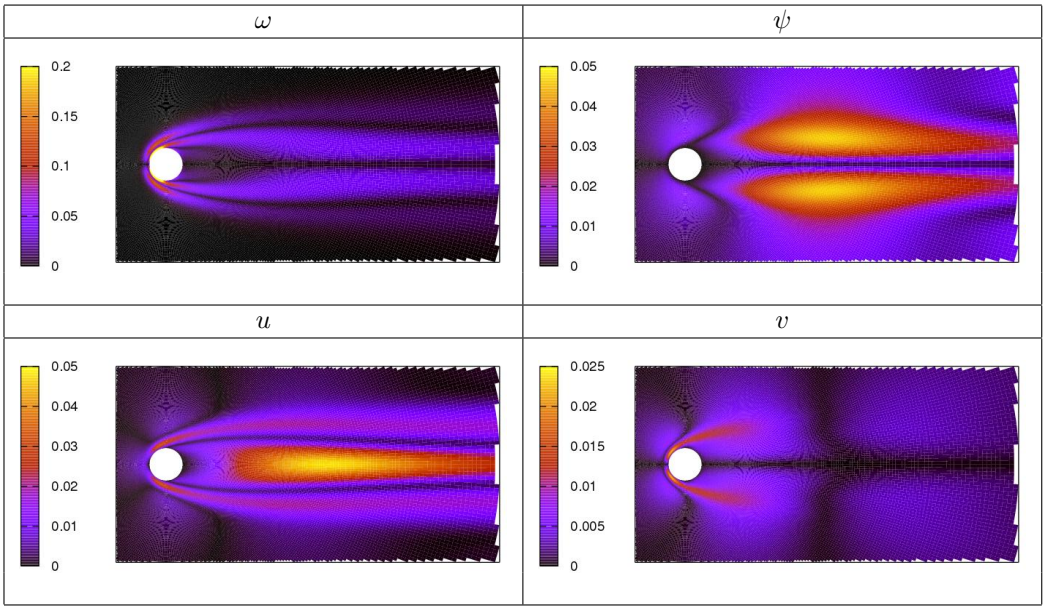

Figure 14: Standard deviation of the vorticity, stream-function and velocity components u (parallel to the inflow) and v (in the transverse direction).

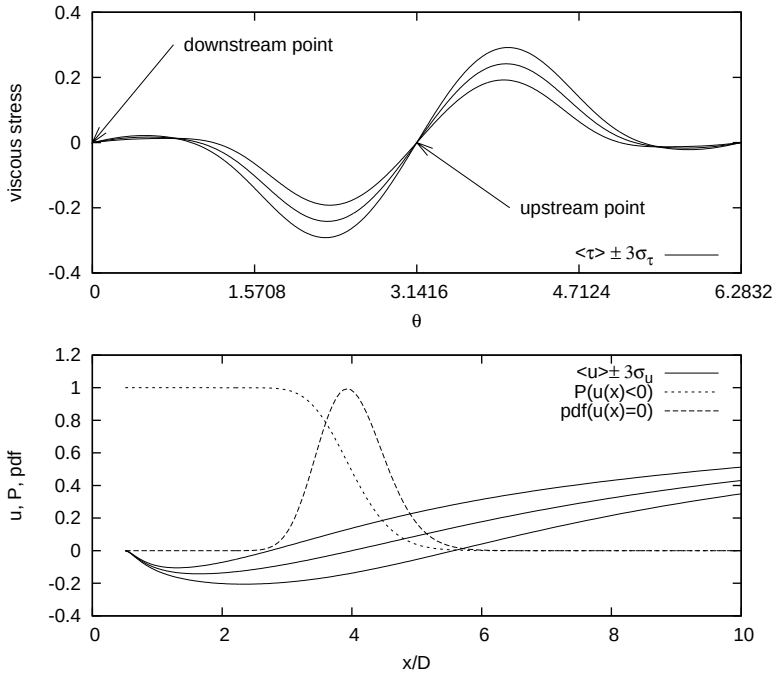

Figure 15: Top plot: representation of the viscous stress distribution along the cylinder boundary using mean value ± 3 standard deviations bounds representation. Bottom plot: mean and ± 3 standard deviations bounds of the longitudinal velocity u, probability of $u < 0$ and probability density of $u = 0$ as a function of the downstream distance x/D from the cylinder center.